Supporting Information

Integrated carbon nanotube and triazine-based covalent organic framework composite for high capacitance performance

Lei Liu, Di Cui, Shuran Zhang, Wei Xie*, Chan Yao, and Yanhong Xu*

Key Laboratory of Preparation and Applications of Environmental Friendly Materials (Jilin Normal University), Ministry of Education, Changchun, 130103, Jilin, PR China.

** Corresponding author*

Email: xiew1415@163.com; xuyh198@163.com

Contents

Section A. Materials and methods

4,4',4''-(1,3,5-Triazine-2,4,6-triyl)trianiline was purchased from Alfa, 2,3,5,6-tetrafluoroterephthalaldehyde was purchased from Sanbang Chemical. All solvents used were purchased from Aladdin.

Fourier transform Infrared (FT-IR) spectra were recorded on a Perkin-elmer model FT-IR-frontier infrared spectrometer. The solid-state UV-visible analyzer was carried out using Jasco V-770 spectrometer (JAPAN) spectrophotometer. Solid-state ^{13}C CP/MAS NMR measurements were recorded using a Bruker AVANCE III 400 WB spectrometer at a MAS rate of 5 kHz and a CP contact time of 2 ms. X-ray photoelectron spectra (XPS) were recorded on an ESCALAB250Xi electron spectrometer (Thermo Fisher Scientific Inc., Waltham, MA, USA). Field-emission scanning electron microscopy (FE-SEM) images were performed on a JEOL model JSM-6700 operating at an accelerating voltage of 5.0 kV. High-resolution transmission electron microscopy (HR-TEM) images were obtained on a JEOL model JEM-3200 microscopy. Powder X-ray diffraction (PXRD) data were recorded on a Rigaku model RINT Ultima III diffractometer by depositing powder on glass substrate, from 2θ = 2.5° up to 40° with 0.02° increment. TGA analysis was carried out using a Q5000IR analyzer (TA Instruments) with an automated vertical overhead thermobalance with a rate of 5 °C min^{-1} under nitrogen atmosphere. Nitrogen sorption isotherms were measured at 77 K with ASIQ (iQ-2) volumetric adsorption analyzer. Before measurement, the samples were degassed in vacuum at 120 °C for more than 10 h. The Brunauer-Emmett-Teller (BET) method was utilized to calculate the specific surface areas and pore volume. The non-local density functional theory (NLDFT) method was applied for the estimation of pore size and pore size distribution.

Electrochemical measurement was carried out in a standard three electrode system with a 1 M H_2SO_4 aqueous solution at 25 °C in a CHI 760 electrochemical work station (CH instrument, USA). Active material (100 μg) coated carbon cloth, Pt wire and a saturated calomel electrodes were considered as working, counter and reference electrodes, respectively. The cyclic voltammograms (CVs) were recorded within a potential window of 0 V to 0.8 V in the scan rate range of 20 to 200 mV s^{-1}. Galvanostatic charge discharge (GCD) activity of electrode material was studied with different constant current density in a

potential window of 0 V to 0.8 V. The electrochemical impedance spectra (EIS) were recorded by applying a sinusoidal perturbation of 5 mV in a frequency domain 0.01 to 10000 Hz.

Calculations of specific capacitance

Based on the GCD data, the gravimetric specific capacitance (C, F g^{-1}) was calculated using the following equation:

$$C = \frac{I \times t}{m \times \Delta V}$$

where I is the discharge current (A), t is the discharge time (s), m is the mass of the active material (g), and ΔV is the potential change during the discharge process (V).

Theoretical calculation

The ground-state geometries of fluorinated and non-fluorinated compounds were calculated with the M06-2X functional and Def2-TZVP basis by using the Gaussian 16 program.

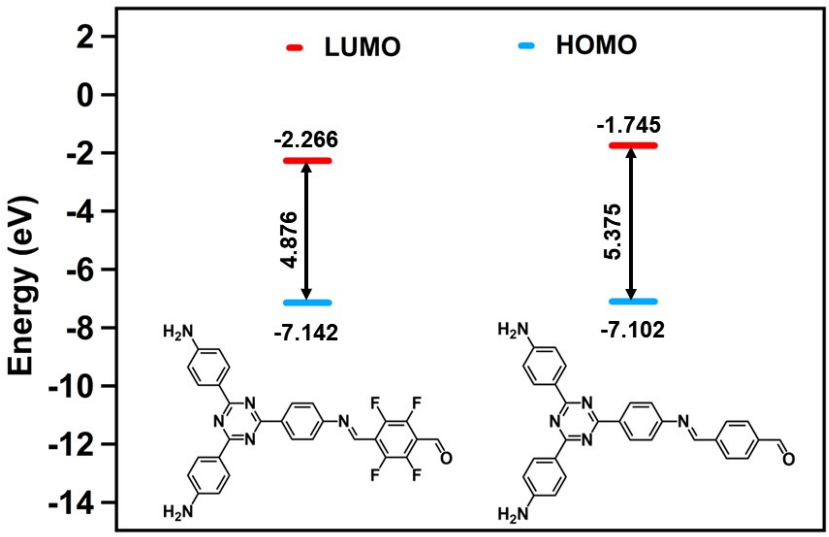

Fig. S1 HUMO and LUMO levels for fluorinated and non-fluorinated compounds.

Section B. Synthetic procedures

Synthesis of TFA-COF

A Pyrex tube was charged with 4,4',4''-(1,3,5-triazine-2,4,6-triyl)trianiline (TAPT, 15 mg, 0.04 mmol) and 2,3,5,6-tetrafluoroterephthalaldehyde (TFA, 13 mg, 0.06 mmol) with a mixed solution of 1,2-dichlorobenzene (o-DCB, 1.5 mL) and n-butanol (n-BuOH, 0.5 mL). An aqueous acetic acid (6 M, 0.2 mL) was used as catalyst. The tube was frozen and vacuumed at 77 K (liquid nitrogen bath), and then sealed with flame. The mixture was heated at 120 °C for 5 days to afford red precipitate, which was isolated by filtration, washed with anhydrous acetone for 5 times, and vacuum drying at 85 °C to afford red powder with 84% isolated yield.

Synthesis of CNT@TFA-COFs

Similar synthetic procedure to TFA-COF. A Pyrex tube was charged with 4,4',4''-(1,3,5-triazine-2,4,6-triyl)trianiline (TAPT, 15 mg, 0.04 mmol), 2,3,5,6-tetrafluoroterephthalaldehyde (TFA, 13 mg, 0.06 mmol) and carbon nanotube (CNT, 2.8 / 9.2 / 14 / 21 mg) with a mixed solution of 1,2-dichlorobenzene (1.5 mL) and n-butanol (0.5 mL). An aqueous acetic acid (6 M, 0.2 mL) was used as catalyst. The tube was frozen and vacuumed at 77 K (liquid nitrogen bath), and then sealed with flame. The mixture was heated at 120 °C for 5 days to afford black precipitate, which was isolated by filtration, washed with anhydrous acetone for 5 times, and vacuum drying at 85 °C to afford black powder with 78-82% isolated yield.

Preparation of TFA-COF and CNT@TFA-COFs electrode materials

The electrode composed of TFA-COF and CNT@TFA-COFs were fabricated by mixing the particular TFA-COF or CNT@TFA-COFs (80%), Super P carbon (10%) and PVDF (10% in N-methyl-2-pyrrolidone) as binder. Spread evenly on carbon cloth and dry at 60 ℃ for 12 h. The typical area and weights of electrode materials are 0.5×0.5 cm^2 and 0.1 mg, respectively.

Section C. Powder X-ray diffraction patterns

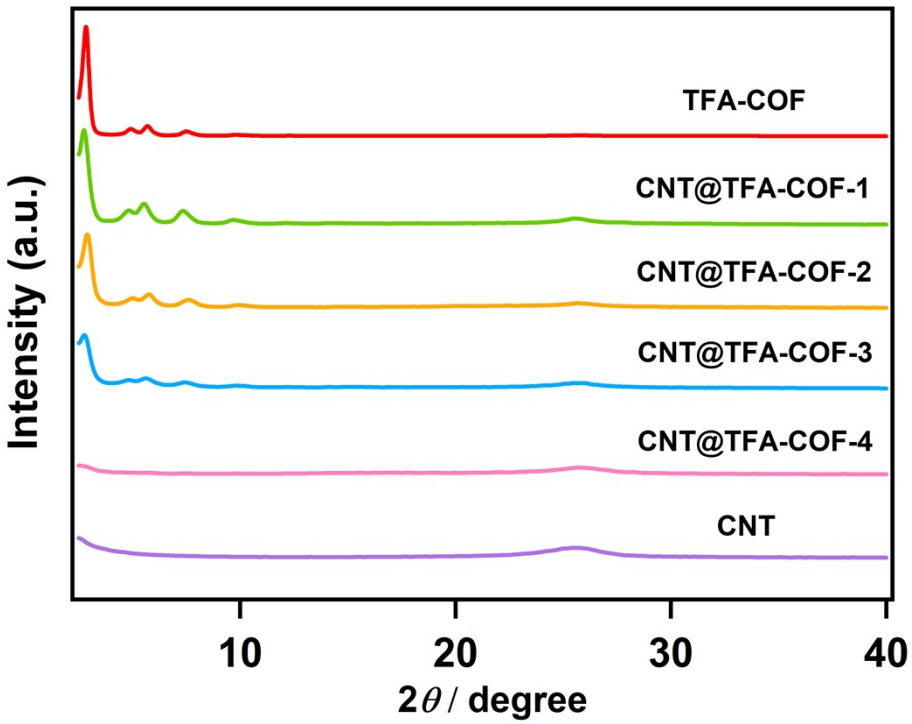

Fig. S2 Powder X-ray diffraction profiles of TFA-COF, CNT and CNT@TFA-COFs.

Section D. The solid-UV spectra

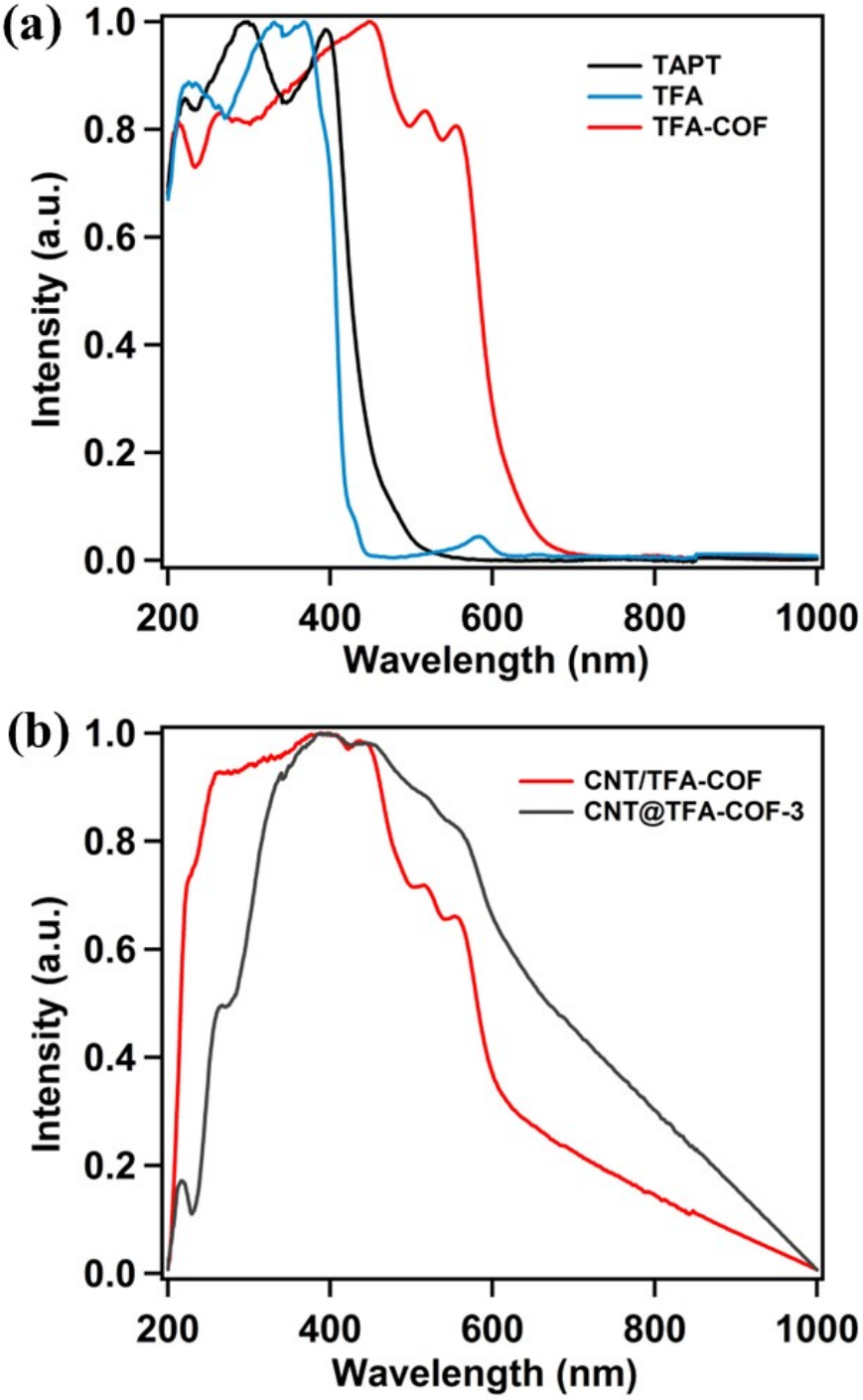

Fig. S3 Solid state UV spectra of (a) TAPT, TFA and TFA-COF; (b) CNT/TFA-COF mixture and CNT@TFA-COF-3 composite.

Section E. SEM images

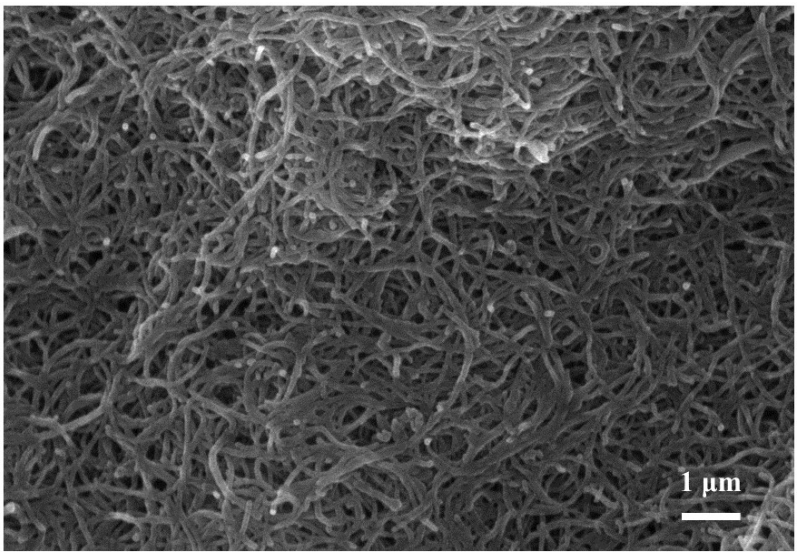

Fig. S4 SEM images of CNT.

Section F. XPS

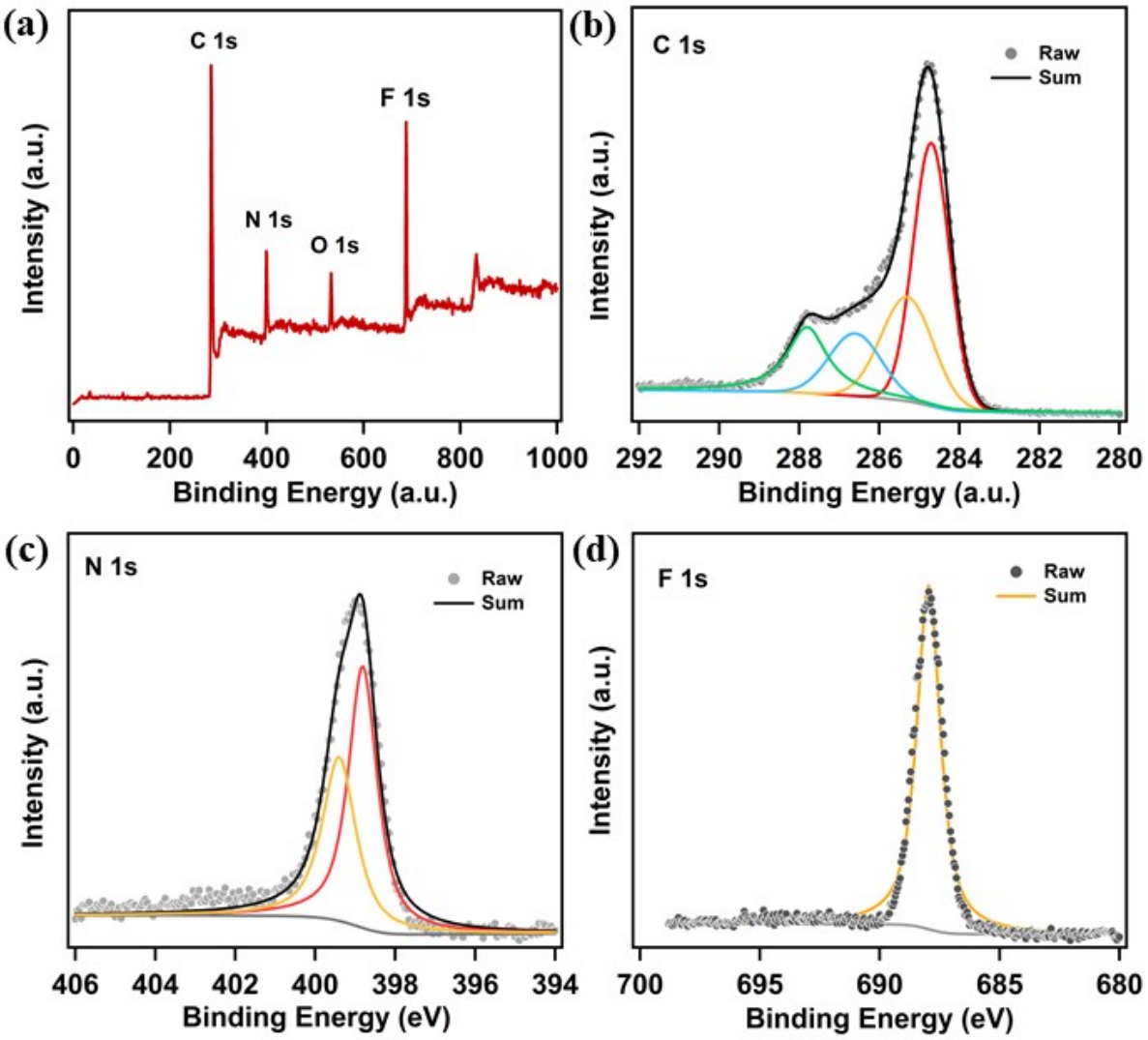

Fig. S5 (a) XPS survey spectra of the TFA-COF. (b) C 1s, (c) N 1s, and (d) F 1s spectra of the TFA-COF.

Section G. N_2 adsorption isotherms

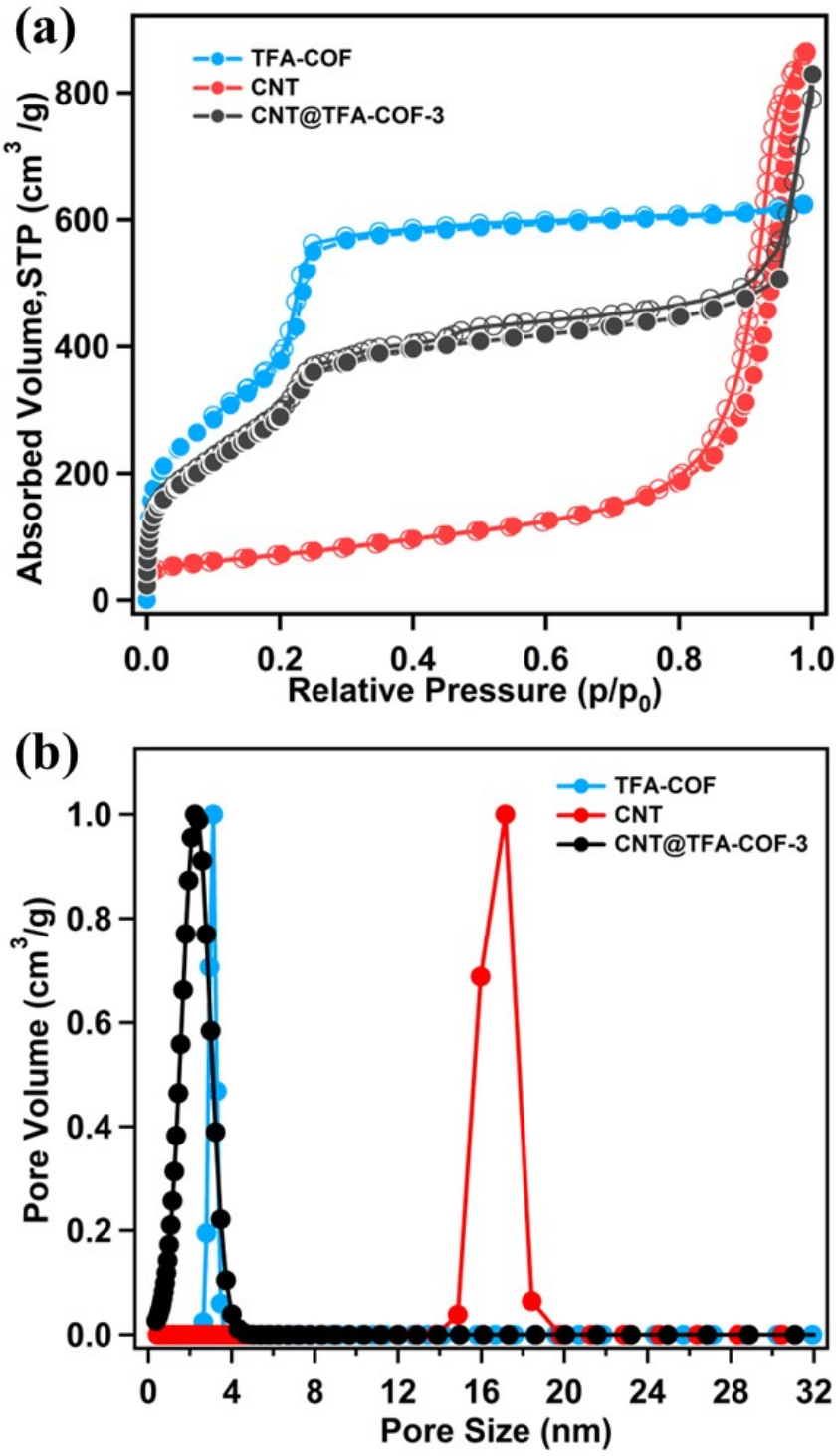

Fig. S6 (a) N_2 adsorption isotherms and (b) pore size distributions of TFA-COF, CNT and CNT@TFA-COF-3 at 77 K.

Section H. Stability

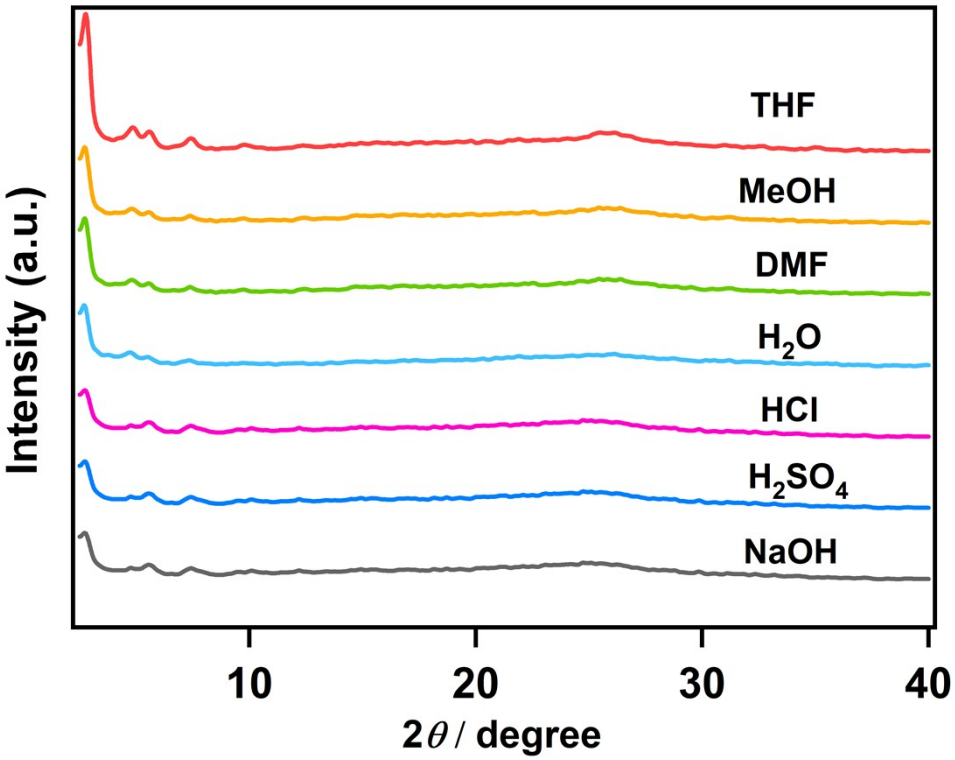

Fig. S7 PXRD patterns of the TFA-COF after soaked in THF, MeOH, DMF, H_2O, HCl, H_2SO_4 and NaOH.

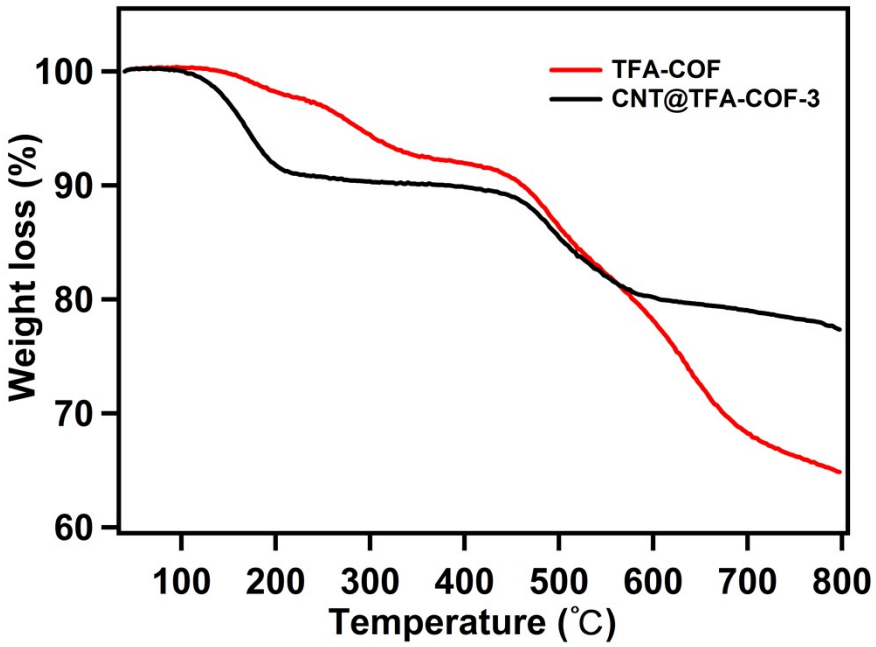

Fig. S8 TGA curves of TFA-COF and CNT@TFA-COF-3.

Section I. Comparison of specific capacitance of CNT@TFA-COF-3 with reported COFs-based supercapacitors in literature

Table S1. Comparison of CNT@TFA-COF-3 with some reported COFs-based specific capacitance.

Polymers	***Specific capacitance* ($F\ g^{-1}$)**	***Current density***	***Electrolyte***	**Refs.**
CNT@TFA-COF-3	338	1 A g^{-1}	1 M H_2SO_4	This work
TpOMe-DAQ	135	0.35 A g^{-1}	3 M H_2SO_4	S1
Dq1Da1Tp	111	1.56 mA cm^{-2}	1 M H_2SO_4	S2
BFTB-PyTA	71	1 A g^{-1}	1 M KOH	S3
TPA-COFs	263.1	0.1 A g^{-1}	1 M H_2SO_4	S4
TaPa-Py COF	209	0.5 A g^{-1}	1 M H_2SO_4	S5
Phos-COF-1	100	1 A g^{-1}	3 M Na_2SO_4	S6
MWCNT@$COF_{TTA–DHTA}$	92.4	0.4 A g^{-1}	1 M Na_2SO_4	S7
NDTT	425.3	0.5 A g^{-1}	1 M KOH	S8
DBT-MA-COF	407	1 A g^{-1}	6 M KOH	S9
rGO-COF-20	321	1 A g^{-1}	1 M H_2SO_4	S10

Section J. Electrochemical study

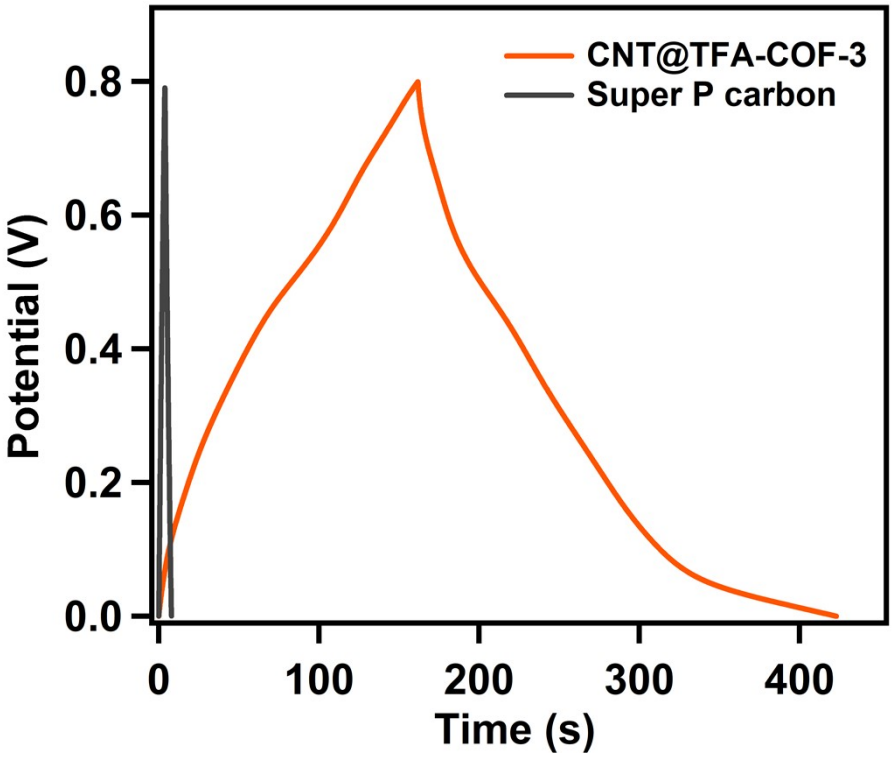

Fig. S9 GCD curves of the CNT@TFA-COF-3 and Super P carbon.

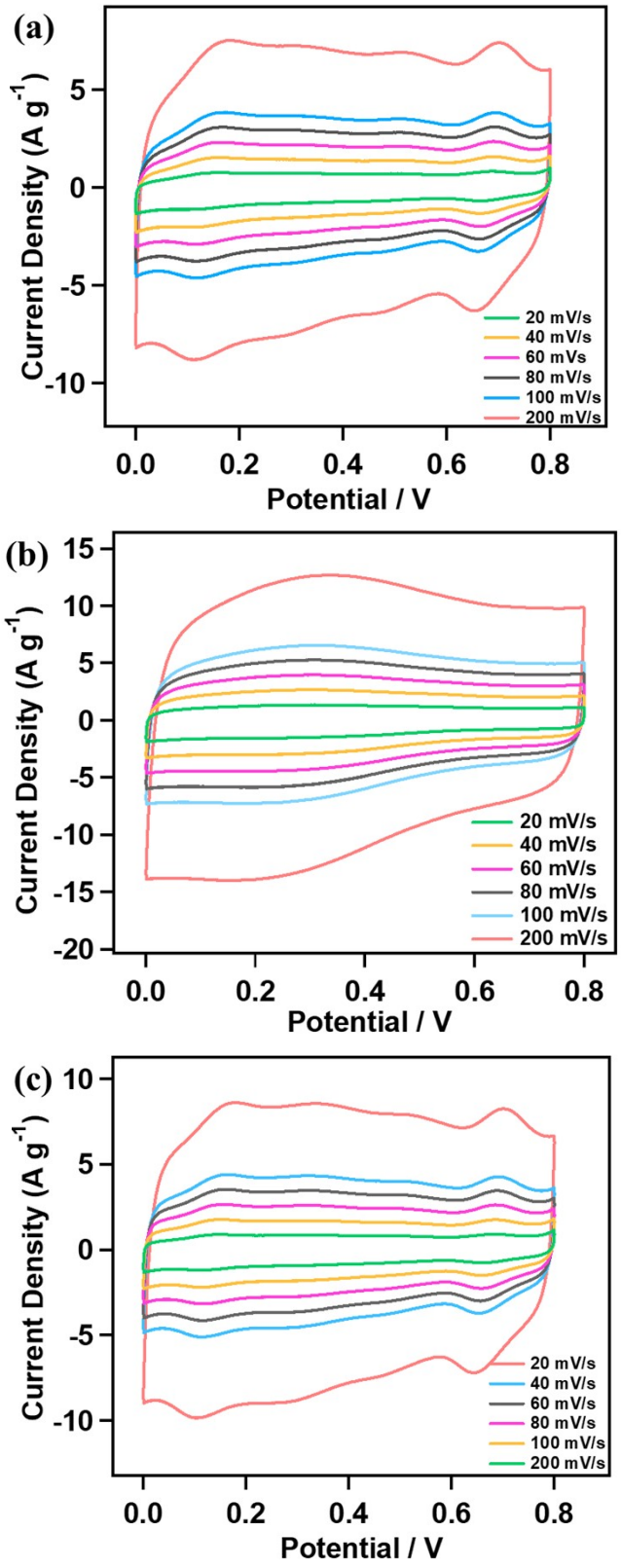

Fig. S10 CV curves of the (a) TFA-COF, (b) CNT, and (c) CNT/TFA-COF mixture.

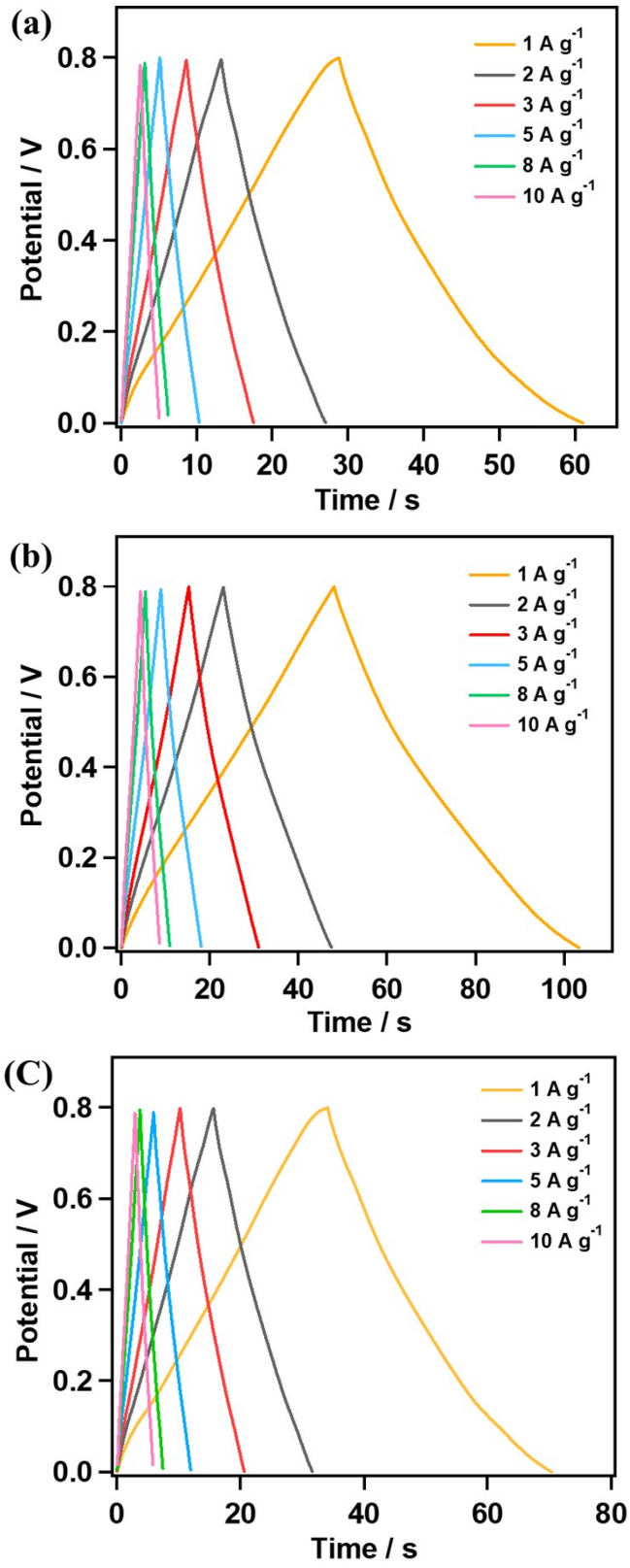

Fig. S11 GCD curves of the (a) TFA-COF, (b) CNT, and (c) CNT/TFA-COF mixture.

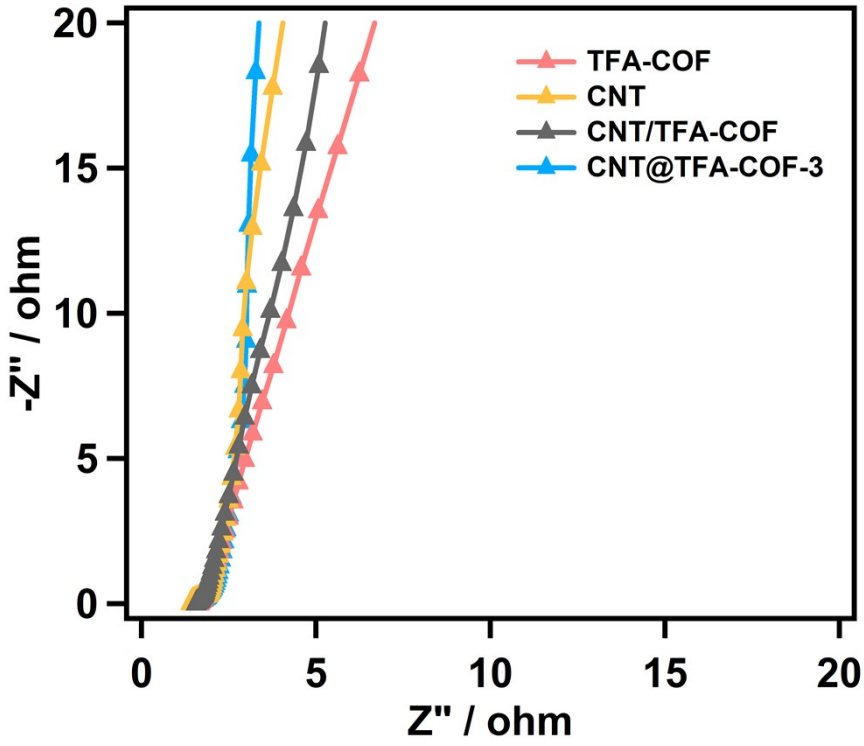

Fig. S12 The nyquist plots of the CNT@TFA-COF-3 composite, TFA-COF, CNT, and the CNT/TFA-COF mixture.

Section K. Supporting references

S1 S. Cai, K. Zhang, J. Tan, S. Wang, S. Zheng, J. Fan, Y. Yu, W. Zhang, and Y. Liu, *ACS Macro Lett*., 2016, **5**, 1348-1352.

S2 A. K. M., V. Vijayakumar, S. Karak, S. Kandambeth, M. Bhadra, K. Suresh, N. Acharambath, S. Kurungot, and R. Banerjee, *ACS Appl. Mater. Interfaces*, 2018, **10**, 28139-28146.

S3 A. F. M. EL-Mahdy, M. B. Zakaria, H. Wang, T. Chen, Y. Yamauch, and S. Kuo, *J. Mater. Chem. A*, 2020, **8**, 5148-25155.

S4 S. Xiong, J. Liu, Y. Wang, X. Wang, J. Chu, R. Zhang, M. Gong and B. Wu, *J Appl Polym Sci*., 2022, **139**, 51510.

S5 A. M. Khattak, Z. A. Ghazi, B. Liang, N. A. Khan, A. Iqbal, L. Li and Z. Tang, *J. Mater. Chem. A.*, 2016, **4**, 16312-16317.

S6 M. Sajjad, R. Tao and L. Qiu, *Journal of Materials Science: Materials in Electronics*, 2021, **32**, 1602-1615.

S7 B. Sun, J. Liu, A. Cao, W. Song and D. Wang, *Chem. Commun*., 2017, **53**, 6303.

S8 C. Weng, X, Li, Z. Yang, H, Long, C. Lu, L. Dong, S. Zhao and L. Tan, *Chem. Commun*., 2022,**58**, 6809-6812.

S9 L. Li, F. Lu, H. Guo and W. Yang. *Mesopor. Mat.,*2021, **312**, 110766.

S10 C. Wang, F. Liu, J. Chen, Z. Yuan, C. Liu, X. Zhang, M. Xu, L. Wei, Y. Chen, *Energy Storage Mater*., 2020, **32**, 448-457.